Please cite this article in press as: Gofman et al., How Does KCNE1 Regulate the Kv7.1 Potassium Channel? Model-Structure, Mutations, and Dynamics of the Kv7.1-KCNE1 Complex, Structure (2012), http://dx.doi.org/10.1016/j.str.2012.05.016

Structure
Article

How Does KCNE1 Regulate the Kv7.1 Potassium Channel? Model-Structure, Mutations, and Dynamics of the Kv7.1-KCNE1 Complex

Yana Gofman,[1] Simona Shats,[2] Bernard Attali,[2] Turkan Haliloglu,[3,4] and Nir Ben-Tal[1,*]
[1]Department of Biochemistry and Molecular Biology
[2]Department of Physiology and Pharmacology
Tel-Aviv University, 69978 Tel-Aviv, Israel
[3]Polymer Research Center
[4]Chemical Engineering Department
Bogazici University, 34342 Bebek-Istanbul, Turkey
*Correspondence: nirb@tauex.tau.ac.il
http://dx.doi.org/10.1016/j.str.2012.05.016

SUMMARY

The voltage-gated potassium channel Kv7.1 and its auxiliary subunit KCNE1 are expressed in the heart and give rise to the major repolarization current. The interaction of Kv7.1 with the single transmembrane helix of KCNE1 considerably slows channel activation and deactivation, raises single-channel conductance, and prevents slow voltage-dependent inactivation. We built a Kv7.1-KCNE1 model-structure. The model-structure agrees with previous disulfide mapping studies and enables us to derive molecular interpretations of electrophysiological recordings that we obtained for two KCNE1 mutations. An elastic network analysis of Kv7.1 fluctuations in the presence and absence of KCNE1 suggests a mechanistic perspective on the known effects of KCNE1 on Kv7.1 function: slow deactivation is attributed to the low mobility of the voltage-sensor domains upon KCNE1 binding, abolishment of voltage-dependent inactivation could result from decreased fluctuations in the external vestibule, and amalgamation of the fluctuations in the pore region is associated with enhanced ion conductivity.

INTRODUCTION

Voltage-dependent ion channels sense changes in the voltage across the cell membrane and respond by allowing specific ions to pass into or out of the cell with high selectivity and efficiency. Among these channels, voltage-dependent potassium (Kv) channels have been the most extensively studied. In excitable cells, such as neurons and muscle cells, the Kv channels allow efflux of K^+ ions across the membrane, maintaining the membrane resting potential. In nonexcitable cells, such as lymphocytes, the Kv channels are the driving force for the entry of Ca^{2+} ions, which are important for the regulation of various cell functions (Cerda and Trimmer, 2010; Yu and Catterall, 2004). The Kv channels consist of four identical monomers with six transmembrane (TM) helices in each. The first four TM helices in each monomer (S1, S2, S3, and S4) form a voltage-sensor domain (VSD), and the last two helices of all subunits (S5 and S6) assemble jointly to form the central pore domain (Figure 1A).

In humans, the Kv7 potassium channel family, encoded by the *KCNQ* genes, comprises five members (Kv7.1–Kv7.5), four of which (Kv7.2–Kv7.5) are expressed in the nervous system (Brown and Passmore, 2009). Kv7.1 is the only family member that is expressed mostly in heart tissues. The main function of Kv7.1 is to repolarize the cardiac cells following the action potential. It accomplishes this function by assembling with KCNE1, a single-TM-segment regulatory subunit. In comparison with the kinetics of the isolated Kv7.1 channel, the KCNE1-Kv7.1 complex manifests slower activation and deactivation of voltage-gated currents (called I_{Ks}) (Jespersen et al., 2005; Van Horn et al., 2011). Mutations in both proteins can lead to cardiac long QT syndrome, which in turn can cause arrhythmias, ventricular fibrillation, and cardiac arrest (Jentsch, 2000; Jespersen et al., 2005; Van Horn et al., 2011).

Despite the biological significance of the Kv7.1-KCNE1 interaction, its exact nature has yet to be elucidated. In fact, even the stoichiometry of the complex remains a subject of debate. Some experiments have shown that two KCNE1 molecules associate with each Kv7.1 tetramer (Chen et al., 2003; Morin and Kobertz, 2008), whereas others point to multiple stoichiometries (Nakajo et al., 2010; Wang et al., 1998). Kang et al. (2008) used a homology model of Kv7.1 (Smith et al., 2007) and the nuclear magnetic resonance (NMR) structure of KCNE1 to predict the structure of the complex. However, our preliminary analysis showed that this model-structure is incompatible with evolutionary data in that the most conserved amino acids of KCNE1 are exposed to the lipid, and the variable residues are buried at the interface with Kv7.1, in contrast to the typical conservation pattern (Figure S1 available online). Therefore, herein we attempt to provide further insight into the Kv7.1-KCNE1 interaction, using the available model-structure of Kv7.1 (Smith et al., 2007) and various computational protein-protein docking techniques in combination with conservation data. To test the structural model, we examined the

Please cite this article in press as: Gofman et al., How Does KCNE1 Regulate the Kv7.1 Potassium Channel? Model-Structure, Mutations, and Dynamics of the Kv7.1-KCNE1 Complex, Structure (2012), http://dx.doi.org/10.1016/j.str.2012.05.016

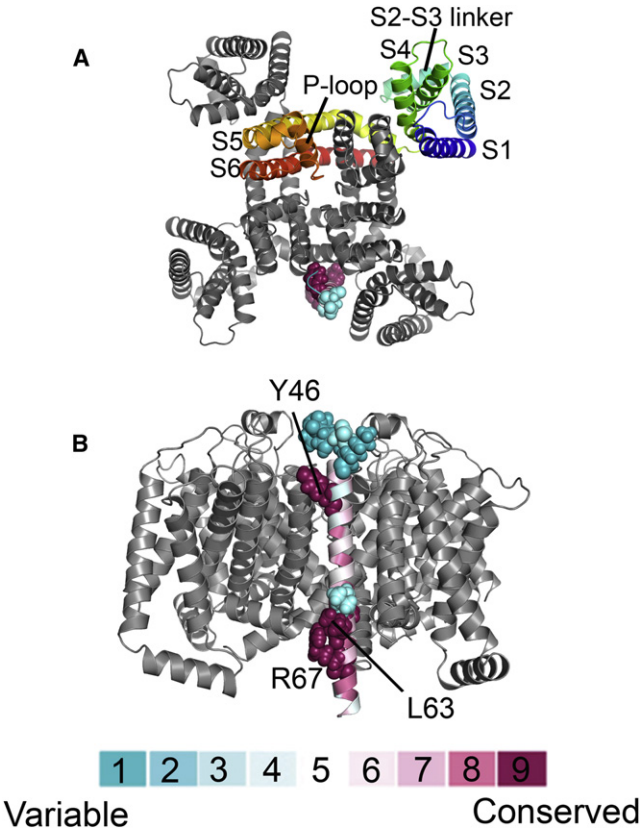

Figure 1. Evolutionary Conservation of KCNE1 within the Complex

In the proposed model, the evolutionarily conserved face of KCNE1 is in contact with the channel, and the variable face points to the lipid bilayer, as it should. The channel tetramer is in gray, and the KCNE1 model is colored by conservation grades according to the color-coding bar, with variable-through-conserved corresponding to turquoise-through-maroon. The most variable residues (scores 1 and 2), namely, R36, S37, S38, D39, G40, K41, and L59, and the most conserved residues (score 9), namely, Y46, I61, L63, R67, and S68, are displayed as space-filled atoms.

(A) Extracellular view. One of the subunits of the homotetrameric channel is presented in rainbow scheme to show the structural elements, and the rest of the subunits are in gray.

(B) Side view. KCNE1 residues Y46, L63 and R67 are marked.

See also Figures S1, S2, S6, and S7.

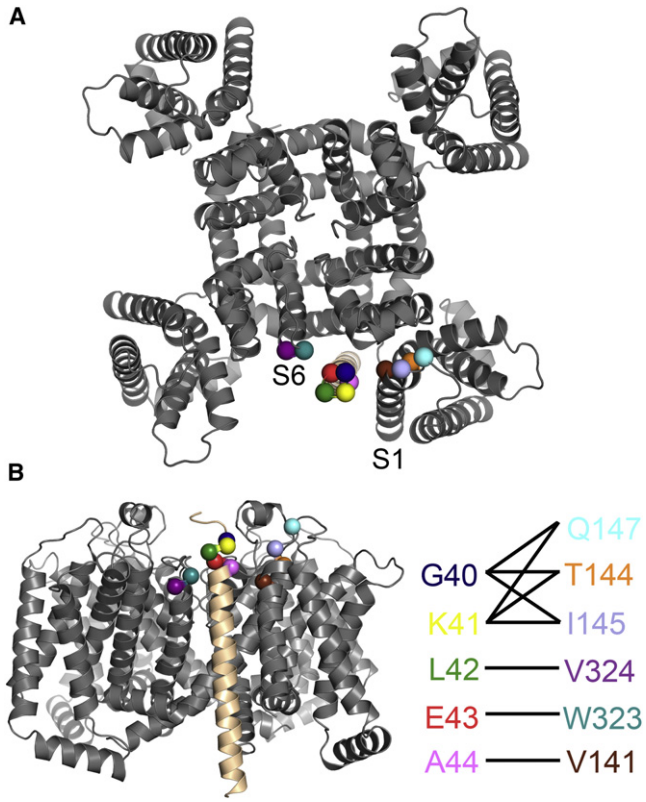

Figure 2. The Model Correlates Well with Disulfide-Link Experiments

(A and B) Extracellular (A) and side (B) views of the model in ribbon representation. KCNE1 appears in light orange and the channel tetramer is in gray. The α-carbons of residues that formed disulfide bonds upon Cys mutation of G40, K41, L42, E43, and A44 in KCNE1, and of V141, T144, I145, Q147, W323, and V324 in the channel are shown as space-filled atoms and colored according to the scheme. The distances between the residue pairs shown here are listed in Table S1. The pairs reported to form S-S bonds when mutated to Cys are connected by solid black lines (Chung et al., 2009; Wang et al., 2011; Xu et al., 2008). In (A), residues 36–39 of KCNE1 are omitted for clarity.

See also Table S1.

electrophysiological properties of Kv7.1 coexpressed with two KCNE1 mutants. Overall, the experimental findings are consistent with our model-structure of the complex.

Our analysis using elastic network models suggests a molecular basis for alterations we observed in the dynamics of the Kv7.1-KCNE1 complex in comparison with the isolated Kv7.1 channel. KCNE1-induced slow deactivation is attributed to the lower mobility of the VSDs of the channel upon KCNE1 association. Abolishment of voltage-dependent inactivation could result from the decreased fluctuations in the external vestibule of the channel upon interaction with KCNE1. Kv7.1 residues D317 and E295 could play a role in the regulation of voltage-dependent inactivation of the channel. KCNE1 association induces changes in the motion of residues G272, V310, and T311 of Kv7.1—changes that could be associated with the channel's enhanced conductivity upon complex formation.

RESULTS

Kv7.1-KCNE1 Complex

We modeled the three-dimensional (3D) structure of an open state of the Kv7.1-KCNE1 complex. The KCNE1 TM helix is not uniformly conserved (Figure S2), and its interface with the Kv7.1 channel is expected to feature conserved amino acids, whereas its lipid-facing region should include variable residues. The model selected on the basis of this criterion (Figure 1) was correlated with experimental data regarding residue pairs that form disulfide bonds when mutated to Cys (Chung et al., 2009; Wang et al., 2011; Xu et al., 2008). Indeed, these residue pairs, located in flexible regions (e.g., loops) in the model-structure, resided at distances of <15 Å from each other and were able to form disulfide links (Careaga and Falke, 1992), supporting the predicted orientation of KCNE1 with respect to Kv7.1 (Figure 2; Table S1). Kang et al.'s (2008) model of the Kv7.1-KCNE1 complex lacks KCNE1 residues 40–44, which prevents us from correlating it with the disulfide data.

Table 1. Matching the Slowest GNM and ANM Modes of the Channel Alone and in Association with KCNE1

	Kv7.1		Kv7.1 + KCNE1	
Motion Type	GNM	ANM	GNM	ANM
I	1,2+3	4	1,2+3	1
II	4	1+2,3	4	3,4
III	5,6+7	6,7+8	5,6+8	5
IV	8	5	7	2

Degenerate modes are separated by commas.

Next, we used our model-structure of the Kv7.1-KCNE1 complex to investigate the effect of KCNE1 association on the intrinsic dynamics of the Kv7.1 channel. To that end, we analyzed the motion of the complex in comparison with the isolated channel using coarse-grained elastic network models, which are not sensitive to atomic details and are suitable for model-structures (Bahar, 2010; Bahar et al., 2010). Elastic network models are capable of exploring large-scale motions related to channel gating and inactivation (Bahar et al., 2010).

Equilibrium Dynamics of the Isolated Channel

We used elastic network models and the available Kv7.1 model-structure (Smith et al., 2007) to investigate global motions of the Kv7.1 channel. The Gaussian network model (GNM) was used to identify the dynamic domains and their cooperative motions. The eight slowest GNM modes of motion of the Kv7.1 tetramer emerged significantly above the rest in the eigenvalue spectrum (Figure S3) and represented the most important contributions to the overall motion of the channel. We analyzed the shapes of the residues' mean-square displacement plots in these modes and identified the minima corresponding to hinge regions that coordinated the motion of dynamic domains in each mode. Hinges often mediate functionally important motions in proteins (Bahar, 2010), and, indeed, the majority of the hinge residues we identified are associated with various disease conditions, such as long QT syndrome and atrial fibrillation (Table S2).

GNM modes 1 and 2 shared the same eigenvalues (Figure S3) and were degenerate. The average shape of the residues' fluctuations in these two modes was very similar to that observed in the third mode (Figure S4). Thus, GNM modes 1–3 correspond to the same motion. Similarly, GNM modes 5–7 represent the same motion. Therefore, we grouped GNM modes 1–8 into four types of motion (Table 1).

We then carried out an anisotropic network modeling (ANM) analysis, which provides information on the directions of the motions in 3D space. We looked for correspondence between the GNM and ANM modes, seeking to link the fluctuations (and correlations between fluctuations) detected by the GNM calculations to their directions, obtained from the ANM analysis. To that end, we compared the distributions of residue fluctuations in each mode (Table 1; Figure S5). We further validated the modes' associations by mapping the GNM-derived cross-correlations between residues on the conformations obtained via ANM (Figures 3, 4A, and 5A).

Motions I and III described alternate slanting of VSD pairs from diagonally opposite monomers toward the pore (Figure 3; Movies S1 and S2). The direction of slanting differed between motions I and III (Movies S1 and S2). Still, in both cases the slanting VSD pushed the external vestibule and P-loop of a neighbor chain toward the pore funnel (Figure 3; Movies S1 and S2). In motion II, the VSDs were swinging, whereas the pore domain appeared to be essentially stationary (Figure 4A; Movie S3). In motion IV, the channel was divided into two dynamic domains connected by hinges located approximately along the membrane mid-plane (Figure 5A; Movie S4). The two domains rotated in opposite directions, with the domain in the intracellular membrane leaflet rotating at significantly lower magnitude.

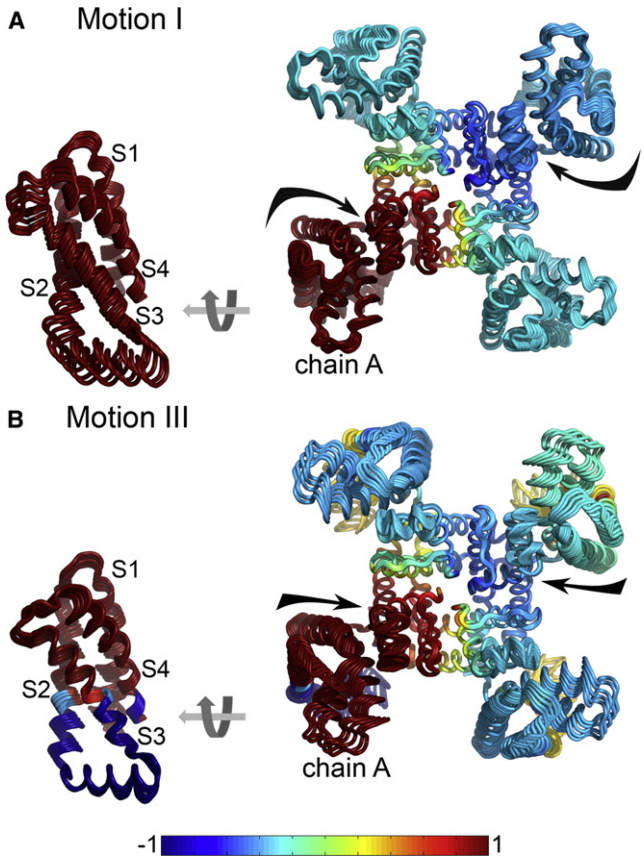

Figure 3. Mapping the Cooperative Dynamics of the Channel on the Conformations Predicted by ANM

The channel is shown in cartoon representation and colored according to the correlation of the chain A paddle with the other residues in the corresponding GNM mode (Table 1). The magnitude of positive and negative correlations between the fluctuations of the residues is color-coded according to the blue-to-red scale at the bottom of the picture. Positive correlation indicates motion of two residues in the same direction, and negative correlation specifies motion in opposite directions. The direction of motion, detected by the ANM analysis, is marked with black arrows. For clarity, the VSDs of chain A are shown in side view as well.

(A) Motion I: Conformations of ANM mode 4, colored according to the corresponding GNM modes 1–3.

(B) Motion III: Conformations of ANM mode 8, colored according to the corresponding GNM modes 5–7. It is apparent that in motion I each VSD domain moves, in essence, as one unit. In motion III, the S1, the N terminus of S2, and the paddle motif (C terminus of S3 and S4 segments) are negatively correlated with the C terminus of S2, the S2-S3 linker, and the N terminus of S3.

See also Movies S1 and S2.

Please cite this article in press as: Gofman et al., How Does KCNE1 Regulate the Kv7.1 Potassium Channel? Model-Structure, Mutations, and Dynamics of the Kv7.1-KCNE1 Complex, Structure (2012), http://dx.doi.org/10.1016/j.str.2012.05.016

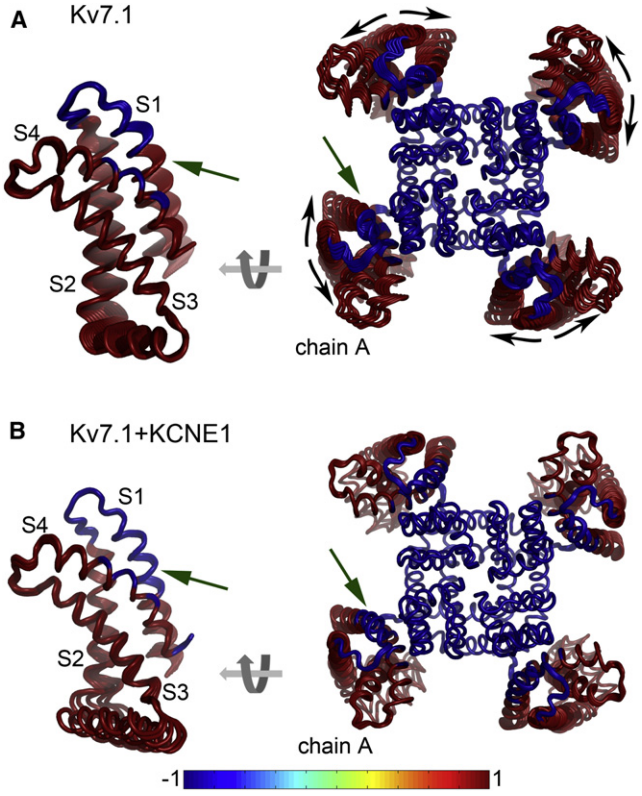

Figure 4. KCNE1 Association Affects the Cooperative Dynamics of Motion II of the Isolated Channel

The conformations are colored according to the correlation of the chain A paddle with the other residues in the corresponding GNM mode (Table 1), using the blue-to-red scale at the bottom.

(A) Channel conformations from ANM mode 1, colored according to the corresponding GNM mode 4. The direction of motion, detected by the ANM analysis, is marked with black arrows.

(B) Averaged conformations of the channel in complex with KCNE1 from ANM modes 3 and 4, colored according to the corresponding GNM mode 4. KCNE1 association affects the cross-correlations of the S1 C terminus (green arrows). See also Movie S3.

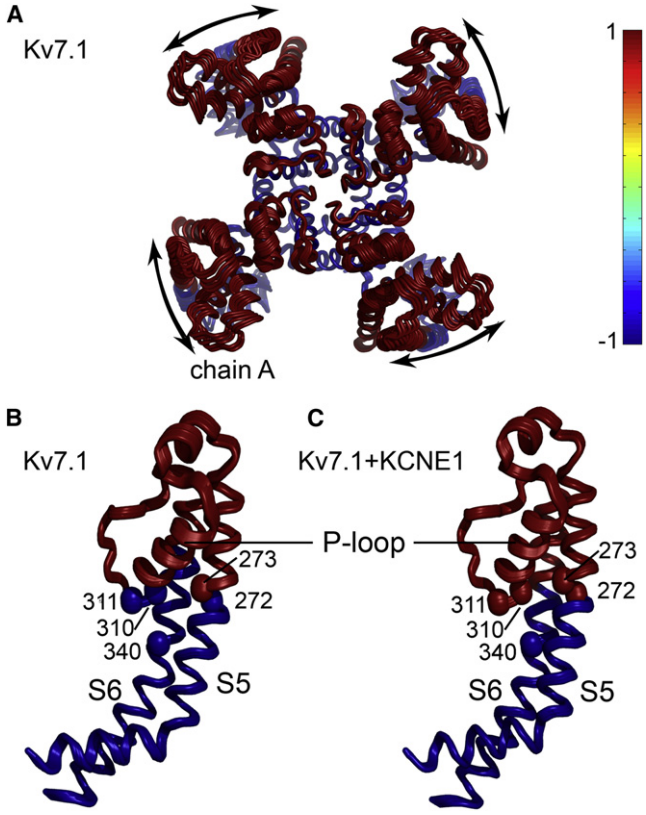

Figure 5. Changes in the Cooperativity Dynamics of Motion IV of the Isolated Channel upon Association with KCNE1

The conformations predicted by ANM are colored according to the correlation of the chain A paddle with the other residues in the corresponding GNM mode (Table 1). The magnitude of positive and negative correlations between the fluctuations of the residues is color-coded according to the blue-to-red scale.

(A and B) Extracellular view of the channel tetramer (A). The direction of motion, detected by the ANM analysis, is marked with black arrows. (A and B) Channel conformations from ANM mode 5, colored according to the corresponding GNM mode 8.

(B and C) Side view of Kv7.1 segments S5 and S6 from a single chain in the absence (B) and presence (C) of KCNE1. The cross-correlations were identical for all four chains. The α-carbons of G272, L273, V310, T311, and F340 are shown as space-filled atoms. Of note, the correlation of residues G272, V310, and T311 with the other residues is reversed upon complex formation. (C) Conformations of the channel in complex with KCNE1 from ANM mode 2, colored according to the corresponding GNM mode 7.

See also Figure S9 and Movie S4.

Equilibrium Dynamics of the Complex

To understand the effect of KCNE1 binding on the channel motion, we conducted GNM and ANM analyses of our model-structure of the Kv7.1-KCNE1 complex. Because the stoichiometry of the complex has not yet been definitively determined, we arbitrarily studied the (tetrameric) channel in complex with four KCNE1 molecules. We then matched the GNM and ANM modes of the complex to the motions of the isolated channel (Table 1; Figure S5). The matching was based mostly on the correspondence of the hinge regions of Kv7.1 in the presence and absence of KCNE1 (Figure S5). Overall, the patterns of the mean-square displacement were essentially preserved upon KCNE1 binding in all four motions and in both elastic models. Complex formation primarily influenced the magnitude of the channel's fluctuations, i.e., the relative mobility of the residues. In addition, the cooperative dynamics of the complex resembled the dynamics of the isolated channel, supporting the match of the GNM and ANM modes in the presence and absence of KCNE1.

A comparison of GNM fluctuations revealed that for the most part, the residue fluctuations were of lower magnitude in the KCNE1-Kv7.1 complex than in the isolated channel (Figure S5). The variations in the magnitude of the ANM fluctuations of the isolated channel versus the complex were more significant than those observed for the GNM fluctuations, especially in motions I, II, and III (Figure S5). The decrease in fluctuation magnitude upon KCNE1 association was manifested mainly in the reduction of VSD fluctuations. In addition, motion III manifested a significant reduction in the fluctuations of the pore domain (Figure S5C). In contrast, the fluctuations of the S2-S3

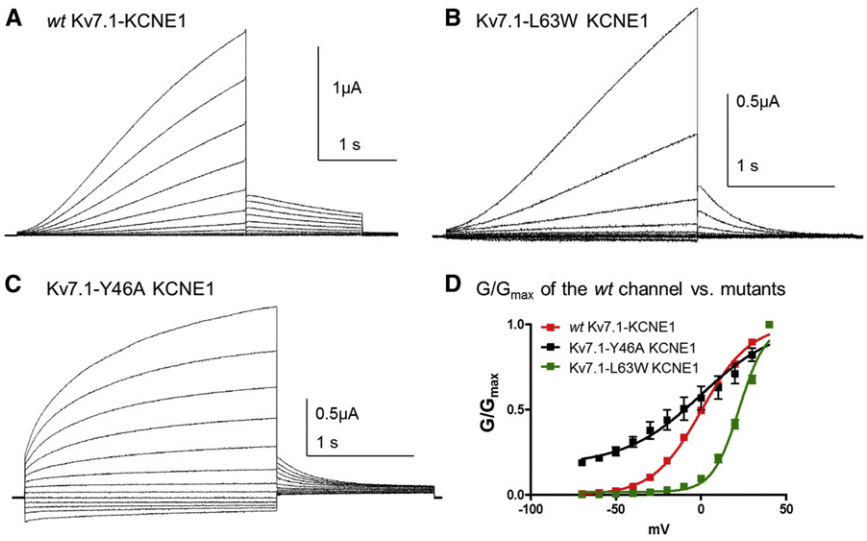

Figure 6. Electrophysiological Properties of the WT Kv7.1-KCNE1 Channel and Two KCNE1 Mutants, L63W and Y46A

(A–C) Representative traces of the WT Kv7.1-KCNE1 (I_{KS}), Kv7.1-L63W KCNE1, and Kv7.1-Y46A KCNE1, respectively, expressed in *Xenopus* oocytes. The currents were recorded from 2.4 s depolarizing pulses of −140 mV to +40 mV, in 15 mV increments, from a holding potential of −80 mV. The tail currents were recorded at −60 mV.

(D) Normalized conductance-voltage relation of the WT Kv7.1-KCNE1, Kv7.1-L63W KCNE1, and Kv7.1-Y46A KCNE1. Voltage-dependent activation curves were fitted by a single Boltzmann function (Equation 6). The error bars mark the standard error of the mean.

linker in motions I, II, and IV increased upon KCNE1 binding (Figure S5).

We also studied the influence of KCNE1 on the cooperative dynamics between structural elements. Whereas only minor alterations were observed in motions I and III, more substantial changes were noted in motion II (Figure 4). In the isolated channel, only a few VSD residues were positively correlated with the immobile pore domain, i.e., were also immobile (Figure 4A). Upon KCNE1 binding, however, a more substantial part of helix S1 was coupled with the pore domain (Figure 4B). Association with KCNE1 also led to variations in the residues' cross-correlations in motion IV, e.g., in G272, V310, and T311, located at the entrance to the selectivity filter (Figure 5). These residues manifested a negative correlation with the rest of the selectivity filter in the isolated channel (Figure 5A) but a positive correlation in the presence of KCNE1 (Figure 5B).

Experimental Data

To probe our structural model, we examined the electrophysiological properties of Kv7.1 coexpressed with two KCNE1 mutants, Y46A and L63W, in comparison with the wild-type (WT) Kv7.1-KCNE1 channel, as described in the Supplemental Information. Y46 and L63 are evolutionarily conserved and located at the outer and inner boundaries of the KCNE1 TM segment, respectively (Figure 1). L63W activated with slower current kinetics compared with the WT complex, as measured by the time of half-maximal activation at +40 mV ($T_{1/2}$ = 1202 ± 95 ms versus $T_{1/2}$ = 952 ± 37 ms, respectively; n = 6–11, $p < 0.05$; Figure 6). In addition, L63W exhibited a faster deactivation rate in comparison with the WT (τ = 336 ± 23 ms versus τ = 1642 ± 134 ms, respectively; n = 6–11, $p < 0.01$) and produced a marked rightward shift in the voltage dependence of channel activation (V_{50} = 22.5 ± 2.3 mV, s = 7.9 ± 1.6 mV versus V_{50} = 0.4 ± 1.5 mV, s = 14.3 ± 1.4 mV, respectively; n = 6–11, $p < 0.01$; Figure 6). In contrast to the L63W mutant, Y46A displayed faster activation kinetics compared with the WT complex, with a significant instantaneous current component ($T_{1/2}$ = 311 ± 32 ms versus $T_{1/2}$ = 952 ± 37 ms, respectively; n = 6–11, $p < 0.01$; Figure 6). Its deactivation kinetics, like those of L63W, were faster than those of the WT (τ = 363 ± 62 ms versus τ = 1642 ± 134 ms, respectively; n = 11, $p < 0.01$). Furthermore, Y46A induced a pronounced left shift in the voltage dependence of channel activation relative to the WT complex (V_{50} = 0.07 ± 0.9 mV, s = 22.5 ± 1.6 mV versus V_{50} = 0.4 ± 1.5 mV, s = 14.3 ± 1.4 mV, respectively; n = 6–11, $p < 0.01$), and even exhibited a voltage-independent component by producing current at voltages negative to E_K (Figure 6). These results suggest that the KCNE1 mutants Y46A and L63W stabilize the open and closed states of the channel, respectively.

DISCUSSION

Limitations of the Calculations

We have presented a 3D model-structure of the Kv7.1 channel in complex with its regulatory unit KCNE1, and correlated it with empirical data. Despite the overall agreement between the model and experimental data (Figure 2), one should keep in mind some inherent limitations of the approach. Because high-resolution structures were not available, we used a homology model of human Kv7.1 (Smith et al., 2007) and an ab initio model of KCNE1. An NMR structure of KCNE1 is available (Kang et al., 2008), but it was determined in micelles and may differ from the structure in a bilayer (Warschawski et al., 2011). Specifically, the helix corresponding to the TM segment displayed a curvature consistent with the micelle radius, and its precise structure within the context of the Kv7.1-KCNE1 complex is still under debate (Coey et al., 2011; Kang et al., 2008). The backbone model of Kv7.1 is expected to be close to the native structure; indeed, it fits the expected evolutionary conservation pattern (Figure S6). In contrast, the KCNE1 model may deviate from the real structure, e.g., in the curvature of the TM segment.

In both of the elastic network models used here, the protein structure is simplified into α-carbons connected by hookean springs of identical force constant (Atilgan et al., 2001; Bahar et al., 1997; Emekli et al., 2008; Haliloglu et al., 1997). Thus, the models do not depend on the identity of the amino acids and the specificity of their interactions. Moreover, the models do not depend on the atomic details of the structure and can

Please cite this article in press as: Gofman et al., How Does KCNE1 Regulate the Kv7.1 Potassium Channel? Model-Structure, Mutations, and Dynamics of the Kv7.1-KCNE1 Complex, Structure (2012), http://dx.doi.org/10.1016/j.str.2012.05.016

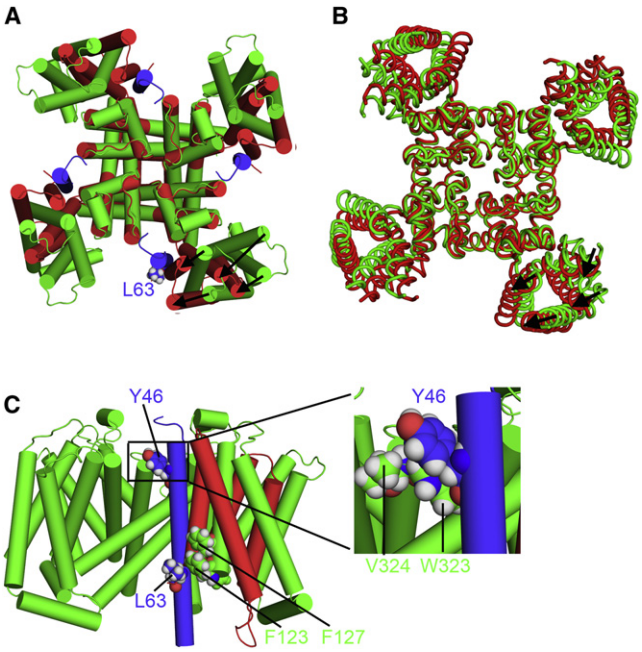

Figure 7. Association of Motion II with Channel Deactivation

(A) Extracellular view of the Kv7.1 model-structure in an open state (colored green) and the closed structure of bacterial potassium channel MlotK1 (colored red) aligned according to the pore domain. Both proteins are shown in cylinder representation. The arrows indicate the possible direction of transition between the open and closed states. The KCNE1 subunits are in blue, and L63 is shown as space-filled atoms.

(B) Kv7.1 conformations as predicted by ANM mode 1 (motion II); only two edge conformations are presented (in red and green). The arrows denote the direction of the motion. The loops connecting S1 and S2, as well as S3 and S4, are omitted for clarity.

(C) Side view of the model-structure of Kv7.1 in the open state (green) and the closed structure of the bacterial potassium channel MlotK1 (red) are aligned according to the pore domain. For clarity, only one VSD of MlotK1 and one KCNE1 subunit are shown. The proteins are shown in cylinder representation. The KCNE1 subunit is in blue, and Y46 and L63 are shown as space-filled atoms. Kv7.1 F123 and F127 are shown as space-filled atoms. The inset shows the tight interface between Kv7.1 S6 and KCNE1. Kv7.1 W323 and V324 are also shown as space-filled atoms.

See also Figure S8.

tolerate small variations in topology (Bahar, 2010; Bahar et al., 2010). This is particularly important in the current study because we used model-structures of both Kv7.1 and KCNE1. Indeed, the magnitude and direction of the Kv7.1 fluctuations presented here are very similar to those observed in previous studies of potassium channels, in which high-resolution structures, still represented using α-carbons only, were used (Haliloglu and Ben-Tal, 2008; Shrivastava and Bahar, 2006; Yeheskel et al., 2010). In particular, our current results regarding Kv7.1 are very similar to those obtained in our earlier analysis of the Kv1.2 channel (Yeheskel et al., 2010), but here we separated modes 4–8 into three motion types instead of investigating them collectively. The two channels share the same fold; in fact, the Kv7.1 model-structure was inferred from the Kv1.2 crystal structure by homology (Smith et al., 2007). Because the two channels share the same architecture, they also manifest very similar amino-acid contact maps, and subsequently most of their hinges are observed in similar structural locations (Table S2). Ligand-gated ion channels also share a similar TM domain and are expected to manifest many of the motions of Kv1.2 and the other voltage-gated channels. However, they also feature the distinctive ligand-binding domain (Yu and Catterall, 2004), which should add unique motions.

Because a protein's intrinsic modes of motion are determined by its architecture, it is possible to predict such conformational changes from the structure only, including those that are dependent on external stimuli such as voltage (Bahar et al., 2010). However, elastic network models approximate only the equilibrium dynamics and may fail to suggest dramatic conformational changes. In what follows, we propose potential functional roles for the channel motions described above and for the effects of KCNE1 on these motions. To consolidate the propositions, we correlate them with experimental data as much as possible.

Lower Mobility of the VSDs in Motion II upon Channel Association with KCNE1 and Slow Deactivation

Motion II mainly describes the fluctuations of the VSDs (Figure 4; Movie S3). The movement of the VSDs is further transmitted to the S4-S5 linkers (Figure S5B; Movie S3), suggesting that it could be related to channel closure and deactivation. To examine this possibility (and in the absence of a structure of a voltage-gated potassium channel), we compared the model-structure of the open state of Kv7.1 that was used here with the crystal structure of the bacterial potassium channel MlotiK1 in its closed state (Clayton et al., 2008). The two channels share a similar fold, although the latter does not display voltage-dependent activity (Nimigean et al., 2004). Of interest, the fluctuations of the VSDs in motion II resemble the transition of Kv7.1 into the conformation captured for the closed state of the MlotiK1 channel (Figures 7A and 7B). This supports the association of motion II with deactivation.

Upon channel association with KCNE1, the magnitude of the VSD fluctuations decreases (Figure S5B). Additionally, in the complex, a more substantial part of the S1 segment is coupled with the immobile pore domain (Figure 4B) as compared with the isolated channel (Figure 4A). Both observations indicate a lower mobility of the VSDs upon KCNE1 association, consistent with the fact that deactivation of the complex is slower than that of the isolated channel (Jespersen et al., 2005; Nakajo and Kubo, 2011).

Molecular Interpretations of the Y46A and L63W Mutants

Overall, the model-structure of the complex manifests the anticipated correlation between the buried versus exposed nature of the amino acids and their evolutionary conservation, namely, KCNE1 residues that are buried at the interface with Kv7.1 are conserved, whereas residues that are exposed to the lipid are variable (Figure 1B). However, the C-terminal extension of the TM helix shows a patch of evolutionarily conserved and exposed residues in close proximity to each other, including L63 and R67 (Figure 1B). Patches of conserved and exposed residues are often important for interaction (Kessel and Ben-Tal, 2010), and we suggest that this patch could fulfill a role in the closed state of the channel. In particular, we suggest that upon deactivation,

the VSD moves toward KCNE1 (Figures 7A and 7C), so that the S1 segment interacts with the conserved patch. All KCNE1 homologs (with the exception of one) feature Leu or Val in position 63 (Figure S7), and the mutation to Trp may promote an aromatic-stacking interaction with F123 and/or F127 of S1 of the channel (Figure 7C). The interaction between these aromatic residues may stabilize the closed state of the channel (Burley and Petsko, 1985). This could explain the observed slow activation and fast deactivation of the channel when it is coexpressed with the KCNE1 L63W mutant (Figure 6) as a shift of the channel population toward the closed state. For comparison, in the model-structure proposed by Kang et al. (2008), L63 is located in a rather tight interface with Kv7.1 S1 (Figure S1), and its mutation to Trp would oppose the movement of S1 (Figure 7) and destabilize the closed state, which should produce the opposite effect, in conflict with the experimental data (Figure 6).

The Y46A mutant showed a different behavior. Electrophysiological studies showed that activation and deactivation in Kv7.1 coexpressed with this KCNE1 mutant were faster than those observed for the WT complex, and comparable to those observed for the isolated Kv7.1 channel (Figure 6C). All KCNE1 homologs feature Tyr or Phe in position 46 (Figure S7). Y46 is tightly packed against the bulky W323 and V324 of the channel (Figure 7C), and replacing it with a small Ala residue would loosen the tight Kv7.1-KCNE1 interface, reducing the regulatory effect of KCNE1. This could explain why the electrophysiological recording of the Y46A mutant resembled that of the isolated channel in activation, deactivation, and even inactivation (Figure 6C). It is noteworthy that Y46, W323, and V324 are all within a cluster of residues that form a hinge in motion II (Table S2; Figure S8), and could be involved in the regulation associated with this motion. In this respect, the observed similarities between the electrophysiological recordings of the Y46A mutant and those of the WT isolated channel (Figure 6C) could be related to deficiencies in motion II. For comparison, in the previous model-structure of the complex, Y46 faces the lipid (Kang et al., 2008), making it difficult to explain the effect of the mutation (Figure S1).

Immobilization of the Pore Region in Motion III and Voltage-Dependent Inactivation

In motion III, pairs of juxtaposed VSDs lean alternately toward the pore (Figure 3; Movies S1 and S2). The resulting distortion in the selectivity filter resembles fluctuations previously associated with inactivation of the prokaryotic channel KcsA (Chakrapani et al., 2011; Cordero-Morales et al., 2006, 2007; Cuello et al., 2010). It was previously demonstrated that KcsA and Kv7.1 share the same inactivation mechanism (McCoy and Nimigean, 2012), and we therefore suggest that motion III is related to Kv7.1 inactivation. Kv7.1 displays two types of inactivation: one is fast and voltage independent, and the other is slow and voltage dependent (Pusch et al., 1998). In motion III, each VSD is divided into two dynamic domains: the first includes the paddle motif, namely, the C terminus of the S3 and S4 segment, S1, and the N terminus of S2; and the second domain includes the C terminus of S2, the S2-S3 linker, and the N terminus of S3 (Figure 3B). The paddle motif is thought to drive conformational changes in response to membrane-voltage variations (Swartz, 2008). In motion III, it is decoupled from the rest of the VSD, and we suggest that this motion is associated with voltage-dependent inactivation.

Upon association with KCNE1, the fluctuations of the external vestibule and P-loop of Kv7.1 are significantly lower compared with those of the isolated channel, especially according to the ANM calculations (Figure S5C). Given that fluctuations of the external vestibule and selectivity filter are essential for inactivation, a decrease in the fluctuations in these regions could indicate dampening, or even elimination, of inactivation. Indeed, one of the known effects of KCNE1 on Kv7.1 is abolishment of voltage-dependent inactivation (Abitbol et al., 1999; Melman et al., 2004; Pusch et al., 1998; Seebohm et al., 2003; Tristani-Firouzi and Sanguinetti, 1998).

D317 and E295 May Play a Role in Voltage-Dependent Channel Inactivation

Previous studies have highlighted the importance of the interaction between residues E71 and D80 for inactivation of the KcsA channel (Figures 8A and 8B) (Chakrapani et al., 2011; Cordero-Morales et al., 2006, 2007; Cuello et al., 2010). These studies demonstrated that electrostatic repulsion between the two residues hindered the approach of the external vestibule toward the funnel and the conformational changes in the selectivity filter region, and that neutralization of either of these residues enhanced inactivation (Cordero-Morales et al., 2006, 2007). Results from previous ANM analyses of KcsA (Haliloglu and Ben-Tal, 2008; Shrivastava and Bahar, 2006) are compatible with these observations because they show that in one of the two most contributing motions, the external vestibules of juxtaposed chains moved toward each other, so that E71 is pulled toward D80 (Haliloglu and Ben-Tal, 2008; Shrivastava and Bahar, 2006). For illustration and comparison, we repeated the ANM studies of KcsA using the HingeProt server (Emekli et al., 2008) (Figures 8A and 8B; Movie S5).

Kv7.1 has a negatively charged residue in position D317, which is equivalent to D80 in KcsA, but a hydrophobic residue in position V308, which is equivalent to E71. Assuming that the inactivation mechanism in Kv7.1 is similar to that in KcsA (McCoy and Nimigean, 2012), we searched for an additional negatively charged residue in the external vestibule of Kv7.1. E295 emerged as a candidate because it is located in the vicinity of D317, and the distance between the α-carbons of D317 and E295 is $\sim$10 Å, which is similar to the distance between the α-carbons of E71 and D80 in KcsA (Cordero-Morales et al., 2007). With regard to the other negatively charged residues in the region, namely, E284, D286, E290, and D301 (Figure 8C), the first three are too distant from D317 to contribute significantly to the repulsion, and D301 is conserved in all Kv7 family members (including Kv7.2), regardless of their inactivation properties. In motion III, E295 approaches D317 when the VSD and external vestibule lean toward the pore funnel (Figures 8C and 8D; Movie S6). Mutation of E295 or D317 to Ala amplifies voltage-dependent inactivation of Kv7.1 (Gibor et al., 2007). Moreover, we examined the sequences of the other Kv7 family members undergoing slow inactivation and observed that Kv7.4 and Kv7.5 each have a negatively charged residue at the position corresponding to E295 (D266 and E294, respectively). The Kv7.2 channel, in contrast, does not undergo inactivation upon depolarization, and features H260 in the equivalent

Please cite this article in press as: Gofman et al., How Does KCNE1 Regulate the Kv7.1 Potassium Channel? Model-Structure, Mutations, and Dynamics of the Kv7.1-KCNE1 Complex, Structure (2012), http://dx.doi.org/10.1016/j.str.2012.05.016

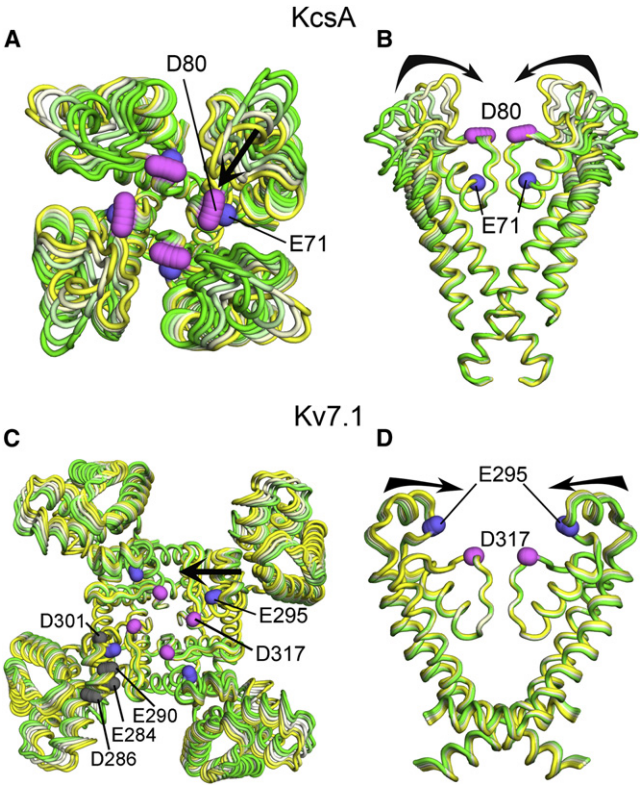

Figure 8. Two Negatively Charged Residues May Affect Slow Voltage-Dependent Inactivation

(A and B) KcsA conformations predicted by the ANM mode related to channel inactivation. The conformations were reproduced with the use of HingeProt (Emekli et al., 2008) and colored according to the direction of motion, ranging from yellow to white and green. The α-carbons of E71 and D80 are shown as blue and pink space-filled atoms, respectively.

(C and D) The conformations predicted by ANM mode 8, related to slow voltage-dependent inactivation in Kv7.1, are colored according to the direction of motion, ranging from yellow to white and green. The α-carbons of E295 and D317 are shown as blue and pink space-filled atoms, respectively. In panel C, the α-carbons of E284, D286, E290, and D301 of one of the chains are shown as gray space-filled atoms.

(A and C) Extracellular view.

(B and D) Side view. For clarity, the pore domains of only two chains are presented.

See also Movies S5 and S6.

position. Thus, we suggest that the electrostatic repulsion between E295 and D317 could hinder voltage-dependent inactivation of Kv7.1, in similarity to the repulsion between E71 and D80 in KcsA.

Changes in the Cross-Correlations in Motion IV and Enhanced Conductivity

The rotation displayed in motion IV has been investigated experimentally and computationally (Haliloglu and Ben-Tal, 2008; Shimizu et al., 2008; Shrivastava and Bahar, 2006; Valadié et al., 2003; Yeheskel et al., 2010), and associated with gating. Roughly speaking, the motion divides the channel into two dynamic domains that rotate in opposite directions around hinges in the membrane mid-plane (Figures 5A and 5B). In the presence of KCNE1, residues G272, V310, and T311 shift from one dynamic domain to another (i.e., change the sense of their cooperative motion), so that all residues in the pore region (and the channel's dynamic domain located in the intracellular membrane leaflet) move together (Figure 5C). With these residues, the pore region rotates as a whole rather than in part, which is expected to increase conductance. This could explain the increased K^+ ion current through the channel upon KCNE1 association (Jespersen et al., 2005), indicating that the three residues mentioned above could be considered as a regulatory switch for enhanced conductivity.

Further support for this notion emerges from the fact that mutation of V310 to Ile in Kv7.1 results in substantially lower currents (Seebohm et al., 2005; Westenskow et al., 2004). V310 and T311 (corresponding to KcsA A73 and T74) are located at the entrance to the selectivity filter and interact with F272 and F273 in S5, and F340 in S6 (corresponding to KcsA V39, L40, and F103; Figures 5B, 5C, and S9). These five residues are involved in channel inactivation, deactivation, and selectivity (Bhate et al., 2010; Cuello et al., 2010; Melman et al., 2004; Panaghie et al., 2006, 2008; Seebohm et al., 2005; Westenskow et al., 2004), and disease-causing mutations in four of them are well known (Smith et al., 2007). Indeed, it was recently suggested that in potassium channels selectivity and inactivation are linked, with F340 in Kv7.1 (or the corresponding position in other channels) and residues interacting with it serving as the link (McCoy and Nimigean, 2012).

Conclusions

We have presented an elastic network analysis of the equilibrium dynamics of our model-structure of the Kv7.1-KCNE1 complex. The model-structure is compatible with the typical evolutionary conservation pattern and with available disulfide mapping studies. Furthermore, it suggests molecular interpretations for electrophysiological phenomena that we observed in the channel coexpressed with two KCNE1 mutants. Our elastic network analysis of the model-structure reveals interesting details with regard to channel deactivation, inactivation, and gating, and suggests important roles for D317 and E295 in channel inactivation and for G272, V310, and T311 in conductivity. Moreover, it enabled us to formulate a mechanistic perspective of how KCNE1 binding may affect channel dynamics. Slow deactivation was attributed to the low mobility of the VSDs upon KCNE1 binding, abolishment of voltage-dependent inactivation resulted from the decreased fluctuations in the external vestibule, and amalgamation of the fluctuations in the pore region was associated with the enhanced conductivity of the channel.

EXPERIMENTAL PROCEDURES

Docking

KCNE1 has an extracellular N terminus, a single TM segment between residues 44 and 66, and a cytoplasmic C terminus (Jespersen et al., 2005; Van Horn et al., 2011). The available 3D structure of human KCNE1 (Protein Data Bank ID 2K21) has a major curve in the TM segment consistent with the radius of the lipid micelles used to determine the structure (Kang et al., 2008). Because the TM conformation may differ significantly from the one observed in micelles (Coey et al., 2011; Warschawski et al., 2011), we modeled the 3D structure of residues 36–75 using the Rosetta Membrane ab initio protocol (Barth et al., 2009). We obtained 10,000 decoys and clustered them, with

a root-mean-square deviation (rmsd) cutoff of 2 Å. The ten lowest-energy candidates in the largest cluster were selected for further analysis. The decoys, all of which were α-helical with a slight kink around residues 56–58, differed from each other in the extent of curvature. We docked these decoys into the symmetric model-structure of the human Kv7.1 (Smith et al., 2007) using PatchDock (Schneidman-Duhovny et al., 2005) and collected the 20 highest-scoring complexes for each candidate. The resulting 200 complexes were filtered manually based on the membrane topology of KCNE1 (Jespersen et al., 2005), and 27 remained. These complexes were evaluated according to their hydrophobicity profiles. The expectation was that hydrophobic residues would be exposed to the lipid, whereas charged and polar amino acids would be buried in the protein core and/or protein-protein interface. We examined each model-structure visually to verify this.

We also evaluated the complexes' evolutionary conservation profiles. We anticipated that evolutionarily conserved amino acids would be buried in the protein core or protein-protein interface, and that variable residues would be exposed to the lipid. We used ConQuass, which assigns scores to model-structures based on the degree to which they adhere to this pattern (Kalman and Ben-Tal, 2010), and constructed the conservation profile using the ConSurf server (Ashkenazy et al., 2010). We collected the homologs from the nonredundant database (Sayers et al., 2011) using PSI-BLAST (Altschul et al., 1997). We then discarded redundant sequences (>99% sequence identity) and aligned the resultant 76 sequences using MUSCLE (Edgar, 2004) (Figure S7). The complex with the highest ConQuass score was chosen for further docking with the Rosetta docking protocol in high-resolution mode (Wang et al., 2007). The 1,000 complexes obtained through this procedure were clustered with an rmsd cutoff of 3 Å and assessed again with ConQuass. The model with the highest ConQuass score from the largest cluster was chosen. As anticipated, in this model, the least conserved face of the KCNE1 helix faces the lipid (Figures 1 and S2).

We also performed independent Kv7.1-KCNE1 docking using the GRAMMX software (Tovchigrechko and Vakser, 2006), and the best model-structure of the complex was essentially the same (data not shown).

The final model-structure of the complex was evaluated against the available data from disulfide mapping studies (Chung et al., 2009; Wang et al., 2011; Xu et al., 2008). In principle, for a disulfide bond to form between a pair of residues, the two residues must be very close to each other, with a Cβ–Cβ distance of ~4.6 Å (Careaga and Falke, 1992; Glaser et al., 2001). However, when the residues are in mobile regions (e.g., loops or helix termini), a bond may form even if the residues are up to 15 Å apart (Careaga and Falke, 1992). The pairs taken into account were G40/T144, G40/I145, G40/Q147, K41/T144, K41/I145, K41/Q147, L42/V324, E43/W323, and A44/V141, where in each pair the first amino acid is from KCNE1 and the second is from Kv7.1 (Chung et al., 2009; Wang et al., 2011; Xu et al., 2008). The distances between the residues in each pair in the final model are listed in Table S1.

Elastic Network Models

We analyzed the Kv7.1-KCNE1 model-structure using elastic network models, as described in the Supplemental Information. These models have provided insights into the dynamics and function of potassium channels (Bahar et al., 2010; Haliloglu and Ben-Tal, 2008; Shrivastava and Bahar, 2006; Yeheskel et al., 2010). For a detailed description of the GNM, see Bahar et al. (1997) and Haliloglu et al. (1997). For details regarding the ANM, see Atilgan et al. (2001) and Emekli et al. (2008).

SUPPLEMENTAL INFORMATION

Supplemental Information includes nine figures, two tables, Supplemental Experimental Procedures, Supplemental References, and six movies, and can be found with this article online at http://dx.doi.org/10.1016/j.str.2012.05.016.

ACKNOWLEDGMENTS

This work was supported by the Israel Science Foundation (Grant 1331/11 to N. B.-T.), State Planning Organization (DPT-2009K120520 to T.H.), Betil Fund (to T.H.), and North Atlantic Treaty Organization (Traveling Grant ESP.CLG 984340 to T.H. and N.B.-T.).

Received: November 10, 2011
Revised: May 29, 2012
Accepted: May 29, 2012
Published online: July 5, 2012

REFERENCES

Abitbol, I., Peretz, A., Lerche, C., Busch, A.E., and Attali, B. (1999). Stilbenes and fenamates rescue the loss of I(KS) channel function induced by an LQT5 mutation and other IsK mutants. EMBO J. *18*, 4137–4148.

Altschul, S.F., Madden, T.L., Schäffer, A.A., Zhang, J., Zhang, Z., Miller, W., and Lipman, D.J. (1997). Gapped BLAST and PSI-BLAST: a new generation of protein database search programs. Nucleic Acids Res. *25*, 3389–3402.

Ashkenazy, H., Erez, E., Martz, E., Pupko, T., and Ben-Tal, N. (2010). ConSurf 2010: calculating evolutionary conservation in sequence and structure of proteins and nucleic acids. Nucleic Acids Res. *38* (Web Server issue, Suppl), W529-33.

Atilgan, A.R., Durell, S.R., Jernigan, R.L., Demirel, M.C., Keskin, O., and Bahar, I. (2001). Anisotropy of fluctuation dynamics of proteins with an elastic network model. Biophys. J. *80*, 505–515.

Bahar, I. (2010). On the functional significance of soft modes predicted by coarse-grained models for membrane proteins. J. Gen. Physiol. *135*, 563–573.

Bahar, I., Atilgan, A.R., and Erman, B. (1997). Direct evaluation of thermal fluctuations in proteins using a single-parameter harmonic potential. Fold. Des. *2*, 173–181.

Bahar, I., Lezon, T.R., Bakan, A., and Shrivastava, I.H. (2010). Normal mode analysis of biomolecular structures: functional mechanisms of membrane proteins. Chem. Rev. *110*, 1463–1497.

Barth, P., Wallner, B., and Baker, D. (2009). Prediction of membrane protein structures with complex topologies using limited constraints. Proc. Natl. Acad. Sci. USA *106*, 1409–1414.

Bhate, M.P., Wylie, B.J., Tian, L., and McDermott, A.E. (2010). Conformational dynamics in the selectivity filter of KcsA in response to potassium ion concentration. J. Mol. Biol. *401*, 155–166.

Brown, D.A., and Passmore, G.M. (2009). Neural KCNQ (Kv7) channels. Br. J. Pharmacol. *156*, 1185–1195.

Burley, S.K., and Petsko, G.A. (1985). Aromatic-aromatic interaction: a mechanism of protein structure stabilization. Science *229*, 23–28.

Careaga, C.L., and Falke, J.J. (1992). Thermal motions of surface alpha-helices in the D-galactose chemosensory receptor. Detection by disulfide trapping. J. Mol. Biol. *226*, 1219–1235.

Cerda, O., and Trimmer, J.S. (2010). Analysis and functional implications of phosphorylation of neuronal voltage-gated potassium channels. Neurosci. Lett. *486*, 60–67.

Chakrapani, S., Cordero-Morales, J.F., Jogini, V., Pan, A.C., Cortes, D.M., Roux, B., and Perozo, E. (2011). On the structural basis of modal gating behavior in K(+) channels. Nat. Struct. Mol. Biol. *18*, 67–74.

Chen, H., Kim, L.A., Rajan, S., Xu, S., and Goldstein, S.A. (2003). Charybdotoxin binding in the I(Ks) pore demonstrates two MinK subunits in each channel complex. Neuron *40*, 15–23.

Chung, D.Y., Chan, P.J., Bankston, J.R., Yang, L., Liu, G., Marx, S.O., Karlin, A., and Kass, R.S. (2009). Location of KCNE1 relative to KCNQ1 in the I(KS) potassium channel by disulfide cross-linking of substituted cysteines. Proc. Natl. Acad. Sci. USA *106*, 743–748.

Clayton, G.M., Altieri, S., Heginbotham, L., Unger, V.M., and Morais-Cabral, J.H. (2008). Structure of the transmembrane regions of a bacterial cyclic nucleotide-regulated channel. Proc. Natl. Acad. Sci. USA *105*, 1511–1515.

Coey, A.T., Sahu, I.D., Gunasekera, T.S., Troxel, K.R., Hawn, J.M., Swartz, M.S., Wickenheiser, M.R., Reid, R.J., Welch, R.C., Vanoye, C.G., et al. (2011). Reconstitution of KCNE1 into lipid bilayers: comparing the structural, dynamic, and activity differences in micelle and vesicle environments. Biochemistry *50*, 10851–10859.

Cordero-Morales, J.F., Cuello, L.G., Zhao, Y., Jogini, V., Cortes, D.M., Roux, B., and Perozo, E. (2006). Molecular determinants of gating at the potassium-channel selectivity filter. Nat. Struct. Mol. Biol. *13*, 311–318.

Cordero-Morales, J.F., Jogini, V., Lewis, A., Vásquez, V., Cortes, D.M., Roux, B., and Perozo, E. (2007). Molecular driving forces determining potassium channel slow inactivation. Nat. Struct. Mol. Biol. *14*, 1062–1069.

Cuello, L.G., Jogini, V., Cortes, D.M., Pan, A.C., Gagnon, D.G., Dalmas, O., Cordero-Morales, J.F., Chakrapani, S., Roux, B., and Perozo, E. (2010). Structural basis for the coupling between activation and inactivation gates in K(+) channels. Nature *466*, 272–275.

Edgar, R.C. (2004). MUSCLE: multiple sequence alignment with high accuracy and high throughput. Nucleic Acids Res. *32*, 1792–1797.

Emekli, U., Schneidman-Duhovny, D., Wolfson, H.J., Nussinov, R., and Haliloglu, T. (2008). HingeProt: automated prediction of hinges in protein structures. Proteins *70*, 1219–1227.

Gibor, G., Yakubovich, D., Rosenhouse-Dantsker, A., Peretz, A., Schottelndreier, H., Seebohm, G., Dascal, N., Logothetis, D.E., Paas, Y., and Attali, B. (2007). An inactivation gate in the selectivity filter of KCNQ1 potassium channels. Biophys. J. *93*, 4159–4172.

Glaser, F., Steinberg, D.M., Vakser, I.A., and Ben-Tal, N. (2001). Residue frequencies and pairing preferences at protein-protein interfaces. Proteins *43*, 89–102.

Haliloglu, T., and Ben-Tal, N. (2008). Cooperative transition between open and closed conformations in potassium channels. PLoS Comput. Biol. *4*, e1000164.

Haliloglu, T., Bahar, I., and Erman, B. (1997). Gaussian dynamics of folded proteins. Phys. Rev. Lett. *79*, 3090.

Jentsch, T.J. (2000). Neuronal KCNQ potassium channels: physiology and role in disease. Nat. Rev. Neurosci. *1*, 21–30.

Jespersen, T., Grunnet, M., and Olesen, S.P. (2005). The KCNQ1 potassium channel: from gene to physiological function. Physiology (Bethesda) *20*, 408–416.

Kalman, M., and Ben-Tal, N. (2010). Quality assessment of protein model-structures using evolutionary conservation. Bioinformatics *26*, 1299–1307.

Kang, C., Tian, C., Sönnichsen, F.D., Smith, J.A., Meiler, J., George, A.L., Jr., Vanoye, C.G., Kim, H.J., and Sanders, C.R. (2008). Structure of KCNE1 and implications for how it modulates the KCNQ1 potassium channel. Biochemistry *47*, 7999–8006.

Kessel, A., and Ben-Tal, N. (2010). Introduction to Proteins: Structure, Function and Motion (Boca Raton: CRC Press).

McCoy, J.G., and Nimigean, C.M. (2012). Structural correlates of selectivity and inactivation in potassium channels. Biochim. Biophys. Acta *1818*, 272–285.

Melman, Y.F., Um, S.Y., Krumerman, A., Kagan, A., and McDonald, T.V. (2004). KCNE1 binds to the KCNQ1 pore to regulate potassium channel activity. Neuron *42*, 927–937.

Morin, T.J., and Kobertz, W.R. (2008). Counting membrane-embedded KCNE beta-subunits in functioning K+ channel complexes. Proc. Natl. Acad. Sci. USA *105*, 1478–1482.

Nakajo, K., and Kubo, Y. (2011). Nano-environmental changes by KCNE proteins modify KCNQ channel function. Channels (Austin) *5*, 397–401.

Nakajo, K., Ulbrich, M.H., Kubo, Y., and Isacoff, E.Y. (2010). Stoichiometry of the KCNQ1 - KCNE1 ion channel complex. Proc. Natl. Acad. Sci. USA *107*, 18862–18867.

Nimigean, C.M., Shane, T., and Miller, C. (2004). A cyclic nucleotide modulated prokaryotic K+ channel. J. Gen. Physiol. *124*, 203–210.

Panaghie, G., Tai, K.K., and Abbott, G.W. (2006). Interaction of KCNE subunits with the KCNQ1 K+ channel pore. J. Physiol. *570*, 455–467.

Panaghie, G., Purtell, K., Tai, K.K., and Abbott, G.W. (2008). Voltage-dependent C-type inactivation in a constitutively open K+ channel. Biophys. J. *95*, 2759–2778.

Pusch, M., Magrassi, R., Wollnik, B., and Conti, F. (1998). Activation and inactivation of homomeric KvLQT1 potassium channels. Biophys. J. *75*, 785–792.

Sayers, E.W., Barrett, T., Benson, D.A., Bolton, E., Bryant, S.H., Canese, K., Chetvernin, V., Church, D.M., DiCuccio, M., Federhen, S., et al. (2011). Database resources of the National Center for Biotechnology Information. Nucleic Acids Res. *39* (Database issue), D38–D51.

Schneidman-Duhovny, D., Inbar, Y., Nussinov, R., and Wolfson, H.J. (2005). PatchDock and SymmDock: servers for rigid and symmetric docking. Nucleic Acids Res. *33* (Web Server issue), W363-7.

Seebohm, G., Sanguinetti, M.C., and Pusch, M. (2003). Tight coupling of rubidium conductance and inactivation in human KCNQ1 potassium channels. J. Physiol. *552*, 369–378.

Seebohm, G., Westenskow, P., Lang, F., and Sanguinetti, M.C. (2005). Mutation of colocalized residues of the pore helix and transmembrane segments S5 and S6 disrupt deactivation and modify inactivation of KCNQ1 K+ channels. J. Physiol. *563*, 359–368.

Shimizu, H., Iwamoto, M., Konno, T., Nihei, A., Sasaki, Y.C., and Oiki, S. (2008). Global twisting motion of single molecular KcsA potassium channel upon gating. Cell *132*, 67–78.

Shrivastava, I.H., and Bahar, I. (2006). Common mechanism of pore opening shared by five different potassium channels. Biophys. J. *90*, 3929–3940.

Smith, J.A., Vanoye, C.G., George, A.L., Jr., Meiler, J., and Sanders, C.R. (2007). Structural models for the KCNQ1 voltage-gated potassium channel. Biochemistry *46*, 14141–14152.

Swartz, K.J. (2008). Sensing voltage across lipid membranes. Nature *456*, 891–897.

Tovchigrechko, A., and Vakser, I.A. (2006). GRAMM-X public web server for protein-protein docking. Nucleic Acids Res. *34* (Web Server issue), W310-4.

Tristani-Firouzi, M., and Sanguinetti, M.C. (1998). Voltage-dependent inactivation of the human K+ channel KvLQT1 is eliminated by association with minimal K+ channel (minK) subunits. J. Physiol. *510*, 37–45.

Valadié, H., Lacapcre, J.J., Sanejouand, Y.H., and Etchebest, C. (2003). Dynamical properties of the MscL of *Escherichia coli*: a normal mode analysis. J. Mol. Biol. *332*, 657–674.

Van Horn, W.D., Vanoye, C.G., and Sanders, C.R. (2011). Working model for the structural basis for KCNE1 modulation of the KCNQ1 potassium channel. Curr. Opin. Struct. Biol. *21*, 283–291.

Wang, C., Bradley, P., and Baker, D. (2007). Protein-protein docking with backbone flexibility. J. Mol. Biol. *373*, 503–519.

Wang, W., Xia, J., and Kass, R.S. (1998). MinK-KvLQT1 fusion proteins, evidence for multiple stoichiometries of the assembled IsK channel. J. Biol. Chem. *273*, 34069–34074.

Wang, Y.H., Jiang, M., Xu, X.L., Hsu, K.L., Zhang, M., and Tseng, G.N. (2011). Gating-related molecular motions in the extracellular domain of the IKs channel: implications for IKs channelopathy. J. Membr. Biol. *239*, 137–156.

Warschawski, D.E., Arnold, A.A., Beaugrand, M., Gravel, A., Chartrand, E., and Marcotte, I. (2011). Choosing membrane mimetics for NMR structural studies of transmembrane proteins. Biochim. Biophys. Acta *1808*, 1957–1974.

Westenskow, P., Splawski, I., Timothy, K.W., Keating, M.T., and Sanguinetti, M.C. (2004). Compound mutations: a common cause of severe long-QT syndrome. Circulation *109*, 1834–1841.

Xu, X., Jiang, M., Hsu, K.L., Zhang, M., and Tseng, G.N. (2008). KCNQ1 and KCNE1 in the IKs channel complex make state-dependent contacts in their extracellular domains. J. Gen. Physiol. *131*, 589–603.

Yeheskel, A., Haliloglu, T., and Ben-Tal, N. (2010). Independent and cooperative motions of the Kv1.2 channel: voltage sensing and gating. Biophys. J. *98*, 2179–2188.

Yu, F.H., and Catterall, W.A. (2004). The VGL-chanome: a protein superfamily specialized for electrical signaling and ionic homeostasis. Sci. STKE *2004*, re15.

